PCCP

ROYAL SOCIETY OF CHEMISTRY

PERSPECTIVE

View Article Online
View Journal | View Issue

Cite this: *Phys. Chem. Chem. Phys.*, 2022, **24**, 21567

Probing combustion and catalysis intermediates by synchrotron vacuum ultraviolet photoionization molecular-beam mass spectrometry: recent progress and future opportunities

Zhongyue Zhou, *[a] Jiuzhong Yang, [b] Wenhao Yuan,[a] Zhandong Wang,[b] Yang Pan [b] and Fei Qi *[a]

Soft photoionization molecular-beam mass spectrometry (PI-MBMS) using synchrotron vacuum ultraviolet (SVUV) light has been significantly developed and applied in various fields in recent decades. Particularly, the tunability of SVUV light enables two-dimensional measurements, *i.e.* mass spectrum and photoionization efficiency spectrum measurements, affording isomer distinguishment in complex reaction processes. Many key intermediates have been successfully detected in combustion and catalysis reactions with the help of the state-of-the-art SVUV-PI-MBMS, promoting the understanding of the chemical mechanisms. Herein, we present a brief review of the instrumentation of beamline and PI-MBMS machines at the current synchrotron user facility Hefei Light Source II and exemplify the advantages of the SVUV-PI-MBMS method with recent applications in combustion and catalysis research, especially in probing key reaction intermediates. Future opportunities with the next generation synchrotron light source and bench-top light source have also been discussed.

Received 26th June 2022,
Accepted 19th August 2022

DOI: 10.1039/d2cp02899a

rsc.li/pccp

1 Introduction

Energy is one of the most important issues in the world as it is the fundamental basis of economy. Fossil energy has been dominating the world's energy consumption for a long time and will remain the most important energy source in the next few decades. Combustion, as the oldest and most important form of energy utilization, provides over 80% of global energy consumption. It is also recognized as the major contributor of air pollutants including CO_2, NO_x, SO_x, polycyclic aromatic hydrocarbons (PAH), fine particles, *etc.*[1] Catalysis is recognized as one of the most important methods in the chemical industry, and it plays a vital role in the production of various chemicals and fuels. The combustion and pollutant formation properties as well as the yield and selectivity of catalytic conversion products are controlled by chemical reactions. To utilize fossil fuels efficiently and cleanly, chemistry knowledge is needed to tailor the combustion or conversion properties and understand the influence of molecular structures of fuels on their homogenous or/and heterogenous reaction mechanisms.

During the combustion and catalytic conversion of fossil fuels, hundreds of species ranging from molecules to radicals can be produced. Convincing chemical mechanism studies of complex reaction processes such as combustion and catalysis cannot be performed without laboratory-scale experimental diagnostics, especially for the measurement of intermediates that are crucial for the reaction network.[2–4] Molecular-beam mass spectrometry (MBMS) is a well-established method capable of measuring both radicals and stable reaction intermediates.[5–7] In the past few decades, photoionization mass spectrometry (PIMS) has had a significant impact on the fundamental understanding of the chemical processes. Since 2003, MBMS with tunable vacuum ultraviolet (VUV) light from synchrotron radiation (SVUV) as an ionization source has been used for combustion studies, including the combustion machines at the Advanced Light Source (ALS) in Lawrence Berkeley National Laboratory[8,9] and Hefei Light Source (HLS) in National Synchrotron Radiation Laboratory (NSRL).[10] More synchrotron-based MBMS methods dedicated to combustion research were later developed at other synchrotron facilities.[11] This method is able to record the intensity of species, not only as a function of the mass-to-charge ratio (mass spectrum), but also as a function of photon energy

[a] *School of Mechanical Engineering, Shanghai Jiao Tong University, Shanghai 200240, P. R. China. E-mail: zhongyue.zhou@sjtu.edu.cn, fqi@sjtu.edu.cn*
[b] *National Synchrotron Radiation Laboratory, University of Science and Technology of China, Hefei, Anhui 230029, P. R. China*

(photoionization efficiency (PIE) spectrum), providing impressive isomer-specific measurement capability.[7,12] In recent decades, the application of SVUV-PIMS method has promoted the development of various fields including reaction kinetics, combustion chemistry,[13–15] catalysis,[16,17] aerosol chemistry,[18] planetary and interstellar chemistry,[19–21] *etc.*

In 2012, the HLS was shut down for upgrading, and a new light source, named HLS-II, was completed and went into operation in decay mode in 2014, and was switched into top-up mode in 2018. During the upgrading period, a new VUV beamline dedicated to combustion research was constructed, covering the energy range of 5–21 eV.[22,23] In this perspective, we will briefly review the instrumental concept of the VUV beamline and the fundamental PIMS method developed since the construction of HLS-II and exemplify the advantages of the SVUV light-based PIMS with recent applications in combustion and catalysis research. In addition, future opportunities with the next generation synchrotron light source and bench-top high brilliant tunable light source will be discussed. We hope that this perspective will serve as a useful roadmap for all researchers who wish to apply these advanced methods in their research, not limited to combustion and catalysis.

2 Instrumentation of the combustion facility at HLS-II

2.1 VUV beamline

Since the ionization energies of a large number of organic molecules (alkanes/hydrocarbons/alkenes/aldehydes, *etc.*) are in the range of 6–12 eV (100–200 nm), the VUV light in this range can directly ionize organic molecules without extensive fragmentation, and the tunability of the light source will afford selectivity during ionization.[25,26] Synchrotron radiation is undoubtedly the most ideal choice. It is a broadband electromagnetic wave emitted when charged particles with a relativistic speed travel in a curved path, which usually occurs in bending magnets, wigglers, or undulators. A beamline is a set of optical elements for delivering light from the synchrotron orbit to experimental endstations. VUV beamlines can be roughly divided into two types, one with a high energy resolution for spectroscopic applications and the other with a medium energy resolution for analytical applications. The combustion beamline (BL03U) at HLS-II is intended to serve as an ionization source for analytical experiments *via* mass spectrometry. As shown in Fig. 1, this beamline is comprised of an undulator, two toroidal mirrors (M1 and M2), two switchable plane gratings (G1/G2), and a multistage gas filter.[22] The centre of the undulator is regarded as the entrance slit, and the broadband radiation from the undulator is collimated horizontally and vertically by M1 with the grazing incidence angle of 7° and then diffracted by G1/G2 with an including angle of 152°. The line densities of G1 and G2 are 200 and 400 l mm^{-1}, covering the photon energy range of 5–14 eV and 10–21 eV, respectively. The diffracted light is then focused by the other toroidal mirror (M2) to the centre of the gas filter, which is located 5000 mm downstream. All optical elements are coated with Au. This simple optical system is advantageous to achieving as high photon flux as possible. As shown in Fig. 2, the photon flux at the end of the beamline is up to 10^{13} photons s^{-1} in the energy range of 6–13 eV and the energy resolution is approximately 4000. The gas filter is comprised of 10 differentially pumped sections, and noble gases such as argon, helium, and neon are filled to eliminate high-order harmonic radiation. Experimental endstations are located about 500 mm downstream from the centre of the gas filter. This layout is beneficial to avoiding contamination of beamline optics by reaction gaseous products from the endstations.

2.2 MBMS

Mass spectrometry with molecular-beam sampling has greatly promoted our fundamental understanding of the chemical combustion processes in the past decades.[5,6,27,28] A typical molecular beam sampling interface consists of a sampling probe and a coaxially mounted skimmer, which is capable to extract gas samples with a free-jet rapid expansion. A collision-free molecular flow can be formed downstream of the skimmer, just like freezing the chemical compositions. For the combination of molecular-beam sampling and mass spectrometry, the resulting molecular beam enters the ionization region, where the compounds are ionized for subsequent mass separation. Fig. 3 shows three examples of the molecular-beam sampling interface used in the recently developed experimental facilities at HLS-II. The first case (Fig. 3a) shows the combination of a pyrolysis reactor with the photoionization mass spectrometer *via* a two-stage MBMS interface.[29] By changing the sampling cones

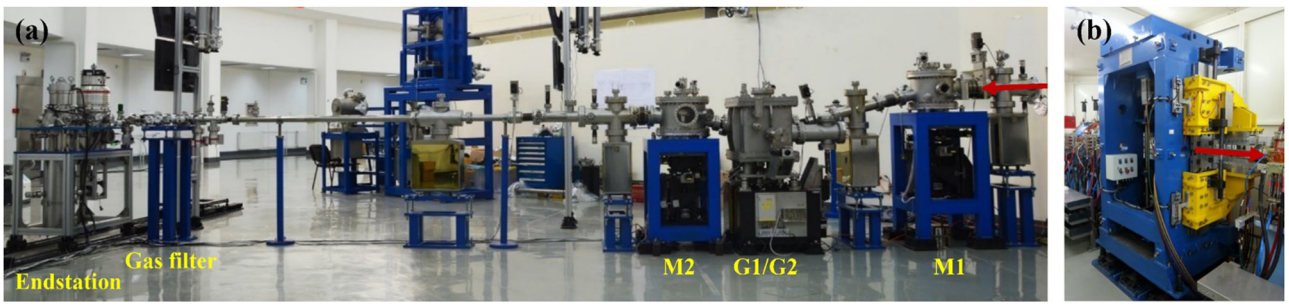

Fig. 1 Photograph of the BL03U beamline[24] (a) and the undulator on the storage ring (b) at Hefei Light Source II. The red arrows denote the direction of light. Adapted and reproduced with permission from the China Academic Journal Electronic Publishing House.

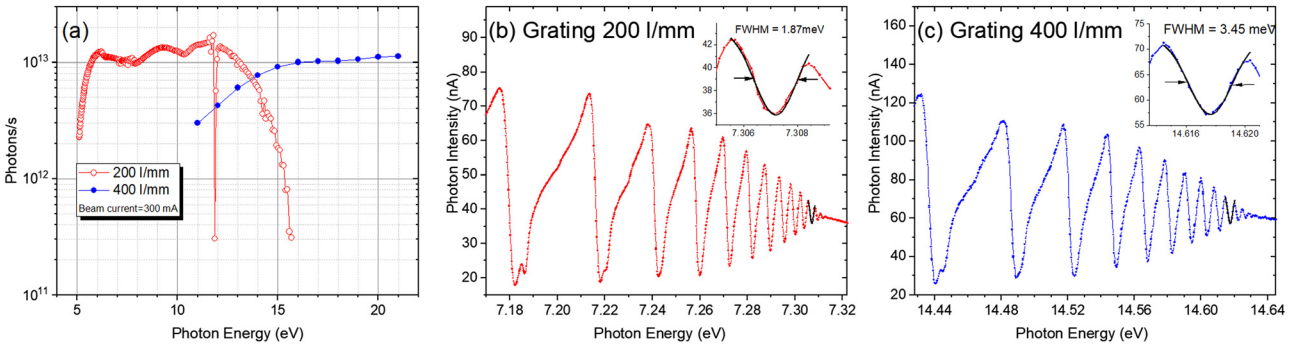

Fig. 2 (a) Photon flux of the combustion beamline at HLS-II, measured by a photodiode located behind the gas filter. The gas filter was filled with argon for the 200 l mm^{-1} grating and neon for the 400 l m^{-1} grating. (b) Energy resolution of the 200 l mm^{-1} grating. (c) Energy resolution of the 400 l mm^{-1} grating. The energy resolution was measured by the adsorption spectra of krypton.[22] Adapted and reproduced with permission from the International Union of Crystallography.

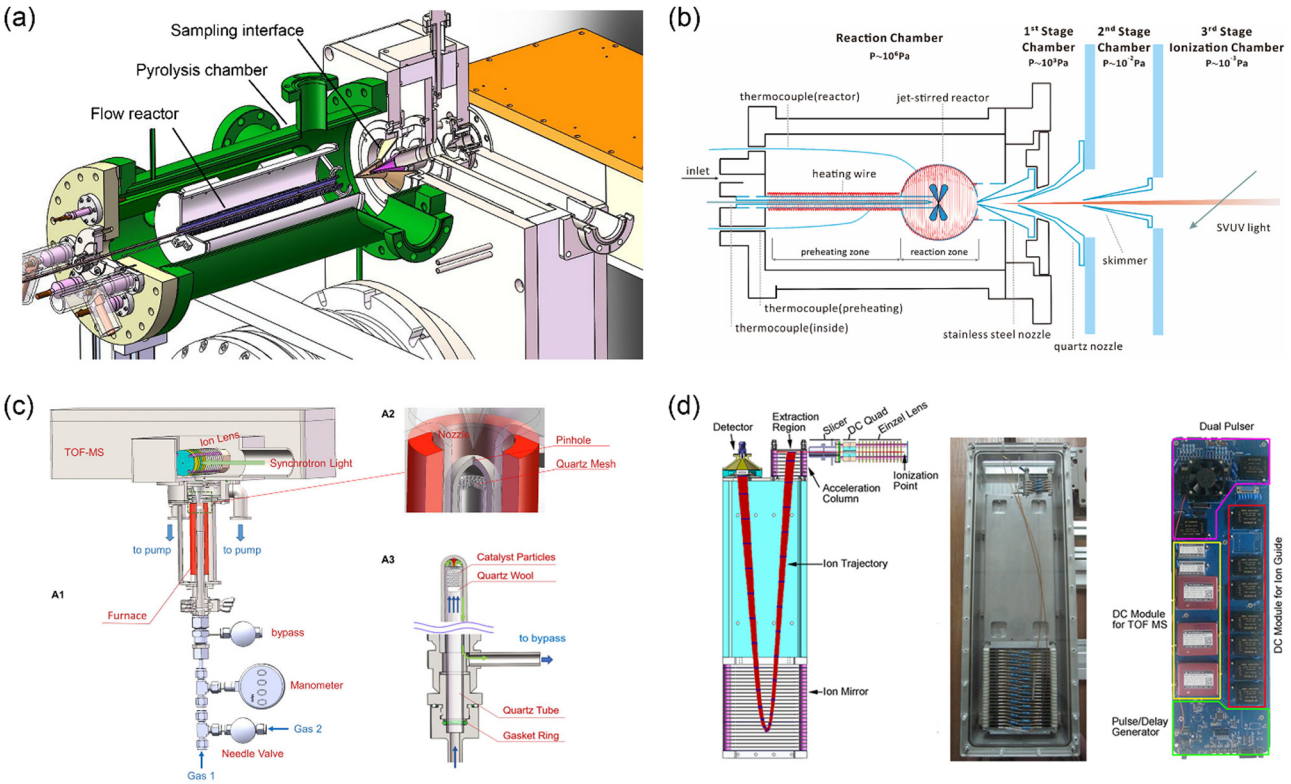

Fig. 3 MBMS apparatus at HLS-II. (a) Pyrolysis reactor combined with PIMS *via* a two-stage sampling interface.[29] (b) High-pressure jet-stirred reactor coupled with PIMS through a three-stage differential interface.[30] (c) High-pressure catalytic reactor coupled to PIMS, A1 is the sketch of the setup, A2 and A3 show the details of the sampling part and the catalytic reactor, respectively.[31] (d) Sketch of the time-of-flight mass spectrometer and the photograph of the assembly and integrated power supply.[22] Adapted and reproduced with permission from Elsevier, the Combustion Institute, AIP, and International Union of Crystallography.

with different aperture sizes to match different reaction pressures, the pressure in the ionization zone can be kept basically constant, so that pyrolysis experiments can be carried out in a wide pressure range from a few Torr to 760 Torr. The second case (Fig. 3b) shows a high-pressure jet-stirred reactor coupled to SVUV-PIMS with a three-stage sampling interface.[30] A stainless-steel nozzle with an orifice diameter of 50 μm is used to withstand the pressures in the reactor (up to 10 bar), and a quartz nozzle and a nickel skimmer are located coaxially downstream, each stage is differentially pumped to form a molecular beam. The quartz reactor cannot act as a pressure-bearing part, instead, a shielding chamber with the same pressure as the reactor is used to balance the pressure difference between the reactor and the external environment. The stainless-steel nozzle is coated with Al_2O_3 to reduce catalytic reactions. The third case (Fig. 3c) presents a high-pressure catalytic reactor coupled to SVUV-PIMS. Different from case 2, to

balance the pressure in the reactor, a small pinhole with an inverted cone angle is placed at the front end of the reactor, which is as close to the sampling nozzle as possible, typically with a distance of approximately 1–2 mm. As reported by You *et al.*, Fischer–Tropsch reactions at pressures up to 1.3 MPa have been achieved successfully.[31]

To facilitate the combination with different reactors, Zhou *et al.*[22] developed a module-designed time-of-flight mass spectrometer. Fig. 3d shows the sketch of the mass analyser as well as the photograph of the assembly and integrated power supply. The mass spectrometer consists of a DC-only ion guide, which is usually located in the ionization chamber of the machines shown in Fig. 3a–c, an acceleration electrode stack with two opposite pulses, a field-free region, a two-stage ion mirror, and a microchannel plate detector. The total length of the mass spectrometer is approximately 600 mm, and the operating frequency is 30 kHz. The mass resolution is approximately 2000, and the limit-of-detection (LOD) is at the level of sub-ppm.

2.3 Qualitative and quantitative measurements

The ion signal of species i recorded *via* MBMS at temperature T and photon energy E can be written as

$$S_i(T,E) = CX_i(T,E)D_i\sigma_i(E)\Phi_p(E)\lambda(k,T,P) \quad (1)$$

where C is the constant of proportionality, X_i is the mole fractions of species, D_i is the mass discrimination factor, $\sigma_i(E)$ is the photoionization cross-section at the photon energy E, $\Phi_p(E)$ is the photon flux, $\lambda(k,T,P)$ is the empirical instrumental sampling function that is the same for all analytes.[32,33]

Because $\lambda(k,T,P)$ is the same for all analytes and mass discrimination factor D_i can be evaluated experimentally, the quantitative information of analytes can be obtained when the corresponding absolute photoionization cross-sections (PICSs) are known. The ionization cross-section is a function of photon energy and represents the efficiency of ionization after interaction with photons. It is a molecule-specific quantity in megabarns (1 Mb = 10^{-18} cm^2). PICSs can be measured experimentally. For example, total PICSs of a few hydrocarbons are measured in the period of 1960s–1990s.[34–37] In recent decades, due to the increasing application of PIMS, the total and partial PICSs for various molecules have been measured by employing synchrotron- or lamp-based PIMS.[38–46] Yang *et al.* established an online database of more than 170 species, including nearly 580 records reported in the literature.[47] Nevertheless, the number of the experimentally determined records for PICSs is still limited; especially for radicals, theoretical calculations of PICSs are often necessary.[48–52] For example, Zhang *et al.*[53,54] reported the calculations of the near-threshold PICSs of molecules including *o*/*m*/*p*-cyanotoluene, benzonitrile, and monocyclic substituted aromatics, providing valuable experience for estimating the PICSs of organic compounds.

When the bulk properties of MBMS are given, the LOD depends on the high photon flux of a synchrotron beamline. The tunability of photon energy enables near-threshold ionization, which usually causes no/less ion fragmentation and offers significantly better selectivity when analyzing a mixture. More importantly, the tunable VUV light allows isomer-specific measurements by scanning the photon energy in a wide range to record the PIE spectra. An example of the PIE spectra is shown in Fig. 4. Note that ethanol and acetaldehyde are unambiguously identified by their ionization energy at 9.33 eV and 10.23 eV, respectively. Quantitative composition of these two isomers was also evaluated by matching the ion signals to the PICS. The solid lines shown in Fig. 4 indicate a mixture of 40% ethenol and 60% acetaldehyde for the 1-butanol and iso-butanol flames, and 20% ethenol and 80% acetaldehyde for the 2-butanol and *tert*-butanol flames. Nevertheless, it should be noted that the number of isomers increases rapidly with molecular weight, and it is extremely challenging to rely solely on PIMS to completely distinguish all isomers.

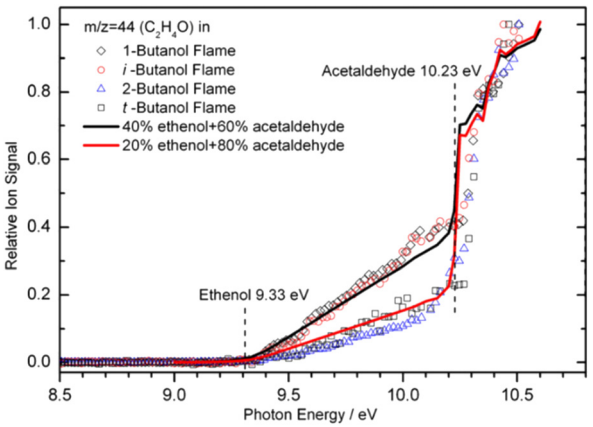

Fig. 4 Photoionization efficiency spectra for m/z 44 recorded in four butanol flames. The flame experiments were conducted with a fuel/oxygen equivalence ratio of 1.71 and the pressure of 30 Torr. The solid lines show the composition of ethanol and acetaldehyde based on their photoionization cross-sections, and dash lines denote the presence of ethanol and acetaldehyde. The matching of the ion signals to the PICS shows the isomeric composition: 40% ethenol and 60% acetaldehyde for the 1-butanol and iso-butanol flames, 20% ethenol and 80% acetaldehyde for the 2-butanol and *tert*-butanol flames.[55] Adapted and reproduced with permission from Elsevier/The Combustion Institute.

3 Combustion chemistry

Comprehensive measurement of intermediates in combustion is essential for the deep understanding of combustion processes. The species measurement results also provide necessary experimental data to validate the detailed kinetic model. The SVUV-PIMS approach has already been used in a great deal of combustion-related experiments, such as laminar premixed flames, laminar flow reactor pyrolysis, jet-stirred reactor oxidation, laminar co-flow diffusion flames, shock tubes *etc.* Herein, we present three examples of SVUV-PIMS in probing intermediates in low-temperature oxidation, heavy PAH precursors, and nitrogenous intermediates, most experiments are conducted at HLS-II.

3.1 Reactive low-temperature oxidation intermediates

Low temperature oxidation is a process involving sequential oxygen addition with the formation of tremendous reactive

species and isomers, which ultimately contribute to two-stage fuel ignition, knocking, and cool flame in internal combustion engines.[3,14] At 2010, a jet-stirred reactor was coupled with MBMS at HLS-I for the first time by Battin-Leclerc and Qi *et al.*[15] and they reported the first direct measurement of alkyl-hydroperoxides and keto-hydroperoxides during the low-temperature oxidation process. This result experimentally examined the conventional two-stage oxygen addition low-temperature oxidation scheme of alkanes, and the experiment supported the assumption made in all the detailed low-temperature oxidation mechanism. In 2016, Wang *et al.*[56,57] observed the highly oxygenated compounds with 4–5 oxygen atoms during alkane low-temperature oxidation with the help of SVUV-PIMS at ALS. A third oxygen addition reaction network was newly proposed and validated to better model autoignition phenomena and reveal the volatile emissions in combustion engines. More recently, the delicate conformational kinetics information during low-temperature oxidation was investigated experimentally based on the observation of alkenal-hydroperoxides and keto-hydroperoxides in low-temperature oxidation of cyclohexane and alkylcyclohexanes.[58–61] Fig. 5a shows a representative mass spectrum recorded in the low temperature oxidation of ethylcyclohexane (ECH) conducted in a jet-stirred reactor.[58] The reaction was conducted with the equivalence ratio (ϕ) of 1.0 at 1 atm and 580 K. The photon energy was fixed at 10.5 eV during spectrum acquisition. A series of reactive intermediates, such as cycloalkylhydroperoxides, keto-hydroperoxides, alkenal-hydroperoxides, and highly oxygenated molecules were detected by SVUV-PIMS. The simulated mole fraction profiles and normalized ion signals shown in Fig. 5b present the formation and decay of these intermediates. The detection of cycloalkylhydroperoxides and keto-hydroperoxides verifies that both the conventional two-stage oxygen addition channels and the recently reported third oxygen addition channels contribute to the low-temperature oxidation of ethylcyclohexane. Conformation-dependent channels are supported by the experimental observations of keto-hydroperoxide and alkenyl-hydroperoxide intermediates.

3.2 PAH precursors

Another nice example of utilizing SVUV-PIMS is the identification of PAH precursors. As PAH is an important emission of combustion and significantly contributes to environmentally hazardous soot particles, chemistry of PAH formation has attracted great interest over the past few decades. The extensive efforts have yielded four chemical mechanisms to explain the formation of PAH, including hydrogen-abstraction acetylene-addition (HACA),[62] hydrogen-abstraction vinylacetylene-addition (HAVA),[63] phenyl-addition dehydrocyclization (PAC),[64] and clustering of hydrocarbons *via* radical chain reactions (CHRCR).[65] However, PAH formation and soot inception processes are not yet fully understood. The formation mechanism of polycyclic aromatic hydrocarbons

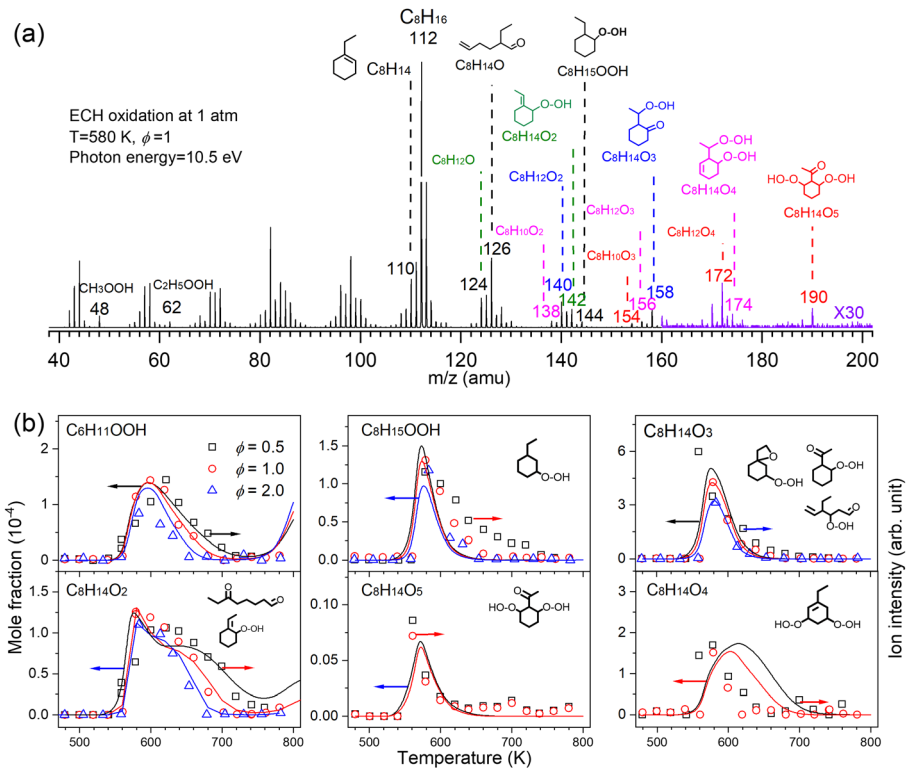

Fig. 5 Important intermediates detected during the low temperature oxidation of ethylcyclohexane (ECH). (a) Mass spectrum recorded at 10.5 eV and 580 K. (b) Mole fraction profiles of highly oxygenated intermediates recorded at 10.0 eV, the symbols represent the normalized ion signals and the lines represent simulation. The oxidation reaction conditions: pressure—1 atm, residence time—2 s, ϕ—0.5, 1.0, 2.0, inlet fuel mole fraction—1%.[58] Adapted and reproduced with permission from Elsevier/The Combustion Institute.

(PAHs) and soot particles is extremely complex with many different types of reactions. In recent years, the application of SVUV-PIMS has previously revealed numerous undetected PAH precursors, especially resonance stabilized radicals whose occurrence may shed further light on specific reaction pathways for the formation of PAHs and soot.

A notable progress is the very recent works reported by Jin and co-workers.[66,67] In the regard of PAH formation, they proposed a radical efficient PAH growth pathway named as CBAC, wherein the propargyl radical reacts with butadiyne to form larger radicals containing newly fused aromatic rings. Fig. 6 illustrates the mass spectrum and PIE curves of critical intermediates undergoing the continuous addition reaction of butadiyne with propargyl.[66] The peak at *m*/*z* 89 (C_7H_5) is likely to represent the fulvenallenyl radical (C_5H_4CCH), which is attributed to a dominant intermediate formed from the additon reaction of butadiyne to propargyl. The fulvenallenyl radical undergoes the H-addition reaction, which yields fulvenallene (C_5H_4CHCH) or its isomers, which generates a peak at *m*/*z* 90. Peaks are also observed at *m*/*z* 139 and *m*/*z* 140, which account for the combined molecular weights of fulvenallenyl (*m*/*z* 89) and butadiyne (*m*/*z* 50). The peak at *m*/*z* 139 ($C_{11}H_7$) is attributed to the product of butadiyne addition to the fulvenallenyl radical, and the signal at *m*/*z* 140 ($C_{11}H_8$) is due to hydrogen addition to $C_{11}H_7$. The proposed CBAC mechanism does not depend on the continuous replenishment of free radicals. For the mechanism of soot inception, they reported the theoretical and experimental identification of key reaction products including phenyl-acenaphthylene, acenaphthylene, phenyl-pyrene, and pyrene in 1-naphthyl/phenyl-acetylene and 4-phenanthryl/phenylacetylene reaction systems, elucidating the self-consistent hydrogen-abstraction phenylacetylene-addition (HAPaA) mechanism.[67]

3.3 Nitrogenous intermediates

Fuel-nitrogen conversion chemistry is an active subject of combustion chemistry research.[68] The prediction of NO_x formation from the combustion of nitrogenous fuels deserves a comprehensive identification of intermediates formed. In addition, as a potential carbon-free fuel, ammonia has attracted great attention in recent years; combustion chemistry of pure ammonia as well as blends of syngas or hydrogen-enriched methane with ammonia deserves renewed attention. During the combustion of nitrogenous fuels and fuel mixtures, different kinds of intermediates can be formed, including not only hydrocarbon intermediates and oxygenated intermediates but also nitrogenous intermediates.[1,68,69] To get a comprehensive understanding of stable products generated, several different diagnostic methods are usually combined to obtain the quantitative information of different products. Recently, SVUV-PIMS has been used to achieve a comprehensive detection of intermediates, especially unstable nitrogenous intermediates produced in the combustion of nitrogenous fuels, ammonia, ammonia/hydrocarbon mixtures and NO_x/hydrocarbon mixtures. For instance, Yuan *et al.*[70] detected dozens of species in the oxidation experiments of propene doped with NO_x, including major products, hydrocarbon intermediates, carbonyl intermediates and nitrogenous intermediates, as shown in Fig. 7. Some critical nitrogenous intermediates were also detected and identified, along with nitrous acid (HONO), nitromethane (CH_3NO_2), 3-nitrosopropene (C_3H_5NO) and 3-nitropropene ($C_3H_5NO_2$). The identification of these species provides key evidence for the direct recombination reactions of alkyl radicals with NO_x, *i.e.* $C_3H_5NO_2$ is the product of the reaction of allyl with NO_2, while CH_3NO_2 is produced from the reaction of CH_3 with NO_2. Moreover, the unambiguous detection of these reactive nitrogenous intermediates of large molecules shed light on the research of interaction chemistry between CH, CHO species and NH_x, NO_x species, which has greatly improved the understanding of the nitrogen chemistry. The methods can be also extended to atmospheric chemistry research, which also involves complex reactions of hydrocarbon species, oxygenated hydrocarbon species and nitrogenous species.

4 Catalysis research

Catalysis is directly applied in around 80% of the production of important industrial chemicals, among which heterogeneous

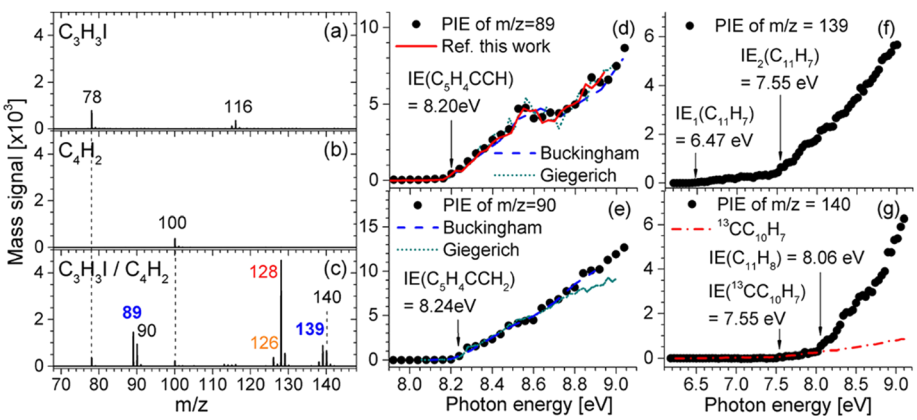

Fig. 6 Photoionization mass spectra and PIE curves of critical intermediates in the C_3H_3I/C_4H_2 reaction. (a) 0.16% C_3H_3I and 99.84% Ar; (b) 16.64% C_4H_2 and 83.36% Ar; (c) 0.16% C_3H_3I, 16.64% C_4H_2, and 83.20% Ar. All mass spectra were obtained at the photon energy of 8.5 eV. PIE curves for (d) *m*/*z* 89, (e) *m*/*z* 90, (f) *m*/*z* 139, and (g) *m*/*z* 140.[66] Reproduced with permission from the American Chemical Society.

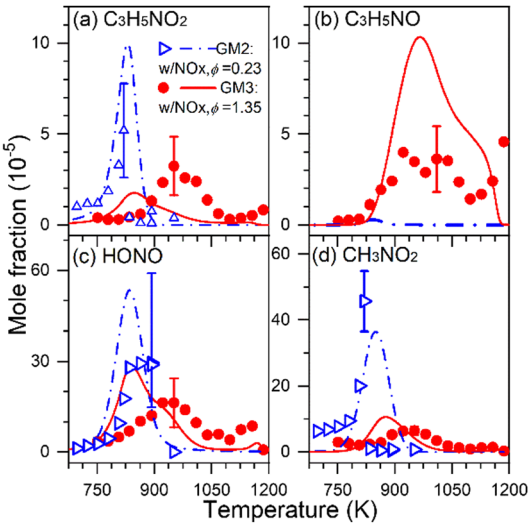

Fig. 7 Experimental (symbols) and simulated (lines) mole fraction profiles of the nitrogenous intermediates in the oxidation of propene/NO_x: (a) 3-nitropropene ($C_3H_5NO_2$), (b) 3-nitrosopropene (C_3H_5NO), (c) nitrous acid (HONO), and (d) nitromethane (CH_3NO_2). A flow reactor with 0.7 cm inner diameter and 22 cm heating length was used, and the average residence time is in between 0.3 and 0.5 s in the investigated temperature range. GM2 represents the gas mixture of propene/NO_x with ϕ = 0.23 and NO/NO_2 ratio = 0.3497; GM3 represents the gas mixture of propene/NO_x with ϕ = 1.35 and NO/NO_2 ratio = 1.782.[70] Reproduced with permission from Elsevier/The Combustion Institute.

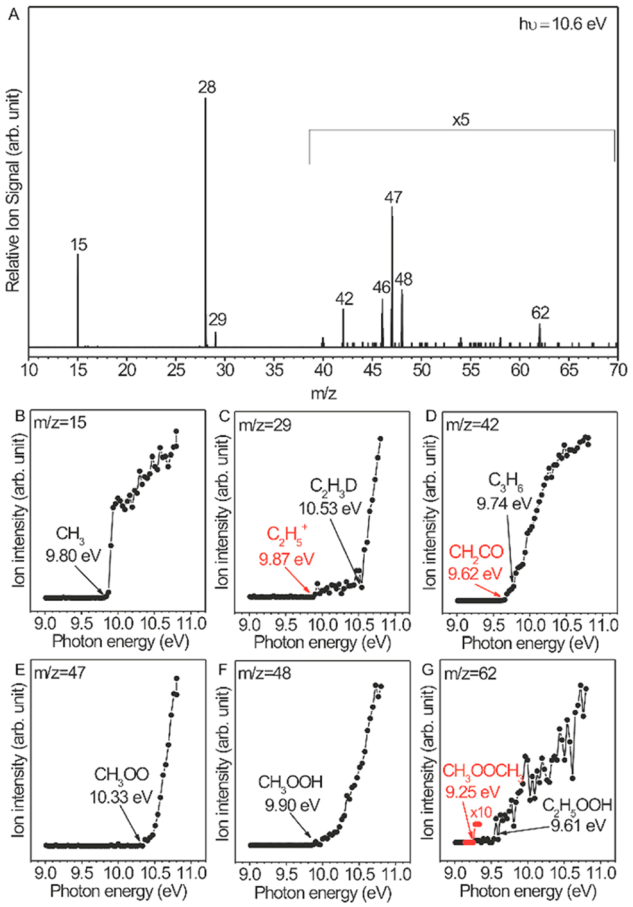

Fig. 8 (A) Gas-phase products of the OCM reaction catalysed by 5.6%-Li/MgO at 750 °C, the mass spectrum was acquired at the photon energy of 10.6 eV and with a catalyst bed of 137 mm obtained from the sampling nozzle of the mass spectrometer. (B–G) Photoionization efficiency spectra of the reactive intermediates.[72] Reproduced with permission from the American Chemical Society.

catalysts are often preferred for their advantages of easier recovery and recycling in industrial production. In addition to the conventionally recognized surface intermediates on the catalysis surface, part of the heterogeneous catalytic reactions also involves reactive and unstable gas-phase intermediates, which are crucial for the fundamental understanding of the catalytic reaction mechanism and guiding the catalyst design. Probing the reactive intermediates of heterogeneous catalytic reactions in the gas phase is challenging, while the recent application of SVUV-PIMS offers a promising approach. The first report is the application of SVUV-PIMS at HLS-I in monitoring the gas phase products in oxidative coupling of methane (OCM) over Li-doped MgO, demonstrating the existence of alkyl radicals as speculated previously.[71] This method shows unique advantages in the process analysis of catalytic reactions, which is further highlighted with recent advances in OCM and oxidative dehydrogenation of ethane (ODHE),[72] syngas conversion,[16] and methanol-to-hydrocarbon (MTH)[17] reactions in the following section.

4.1 Gas-phase reactive radicals in OCM and ODHE reactions

OCM has attracted great interest because of its potential to produce value-added products from natural gas, biogas, *etc.* Mechanistic investigation of OCM reactions is necessary for developing efficient catalysts and designing proper reactors. A radical-involved mechanism has been proposed,[73–76] but there is a lack of experimental evidence for radicals such as ethyl radicals and peroxide radicals due to their high reactivity and very low concentration. This study is far from a comprehensive understanding of the mechanism. Distinct progress is the direct measurement of a series of gas-phase reactive intermediates including methyl radicals, ethyl radicals, methyl peroxide radicals, ethyl peroxide radicals, methyl hydroperoxide, and ethyl hydroperoxide during OCM and ODHE reactions over Li/MgO catalysts.[72] Fig. 8A shows the photoionization mass spectrum of the OCM products on the basis of 5.6%-Li/MgO at 750 °C. This mass spectrum was recorded at a photon energy of 10.6 eV, which is sufficient to get the molecule–ions of the intermediates. The assignment of reactive intermediates was further confirmed with PIE spectra (Fig. 8B–G), especially the peroxide radicals that have long been considered as important intermediates in OCM reactions. Similar radicals were also observed in ODHE reactions.[72] Secondary reactions of these reactive intermediates in the gas phase are also elucidated by adjusting the distances between the catalyst bed and the molecular-beam sampling nozzle. These observations greatly improved the understanding of OCM and ODHE mechanisms.

4.2 Key intermediates in syngas conversions

Another interesting application of SVUV-PIMS is probing the key intermediate, ketene, in syngas (CO + H_2) conversion.

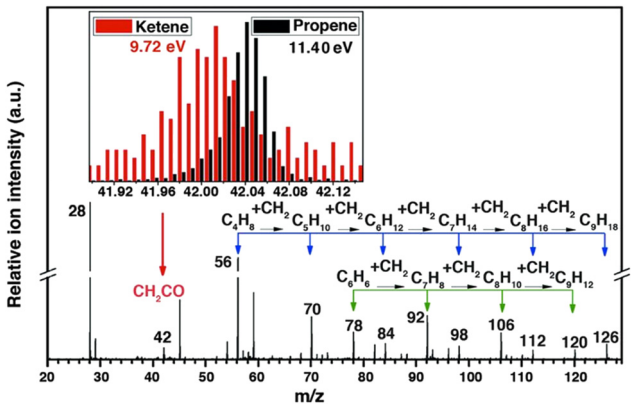

Fig. 9 Photoionization mass spectrum of products in syngas conversion over $ZnCrO_x$ by SVUV-PIMS at 9.72 eV. The insets display the signals of m/z = 42.01 (ketene) and m/z = 42.05 (propene) detected at 9.72 and 11.40 eV, respectively.[16] Adapted and reproduced with permission from AAAS.

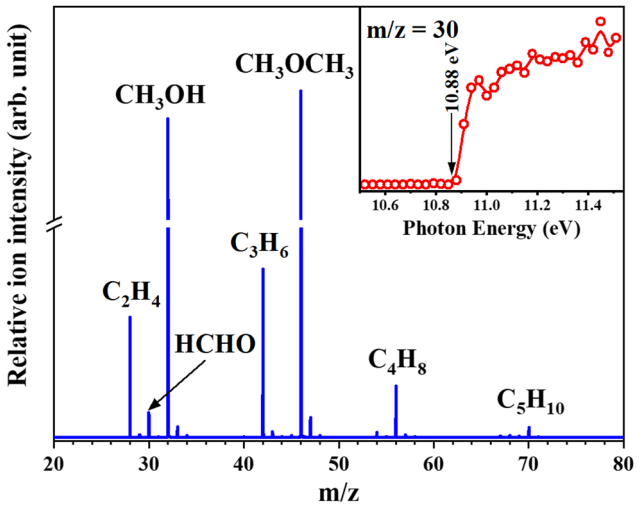

Fig. 10 Photoionization mass spectrum of the products of the MTH process recorded at 11.0 eV. The inset shows the PIE spectrum of the product with m/z 30.[17] Reaction conditions: HSAPO-34 was used as a catalyst; the reaction temperature was 450 °C; the pressure was 2 Torr; the methanol weight hourly space velocity was 11.74 $g_{methanol}\ g_{catalysts}^{-1}\ h^{-1}$. Adapted and reproduced with permission from Wiley-VCH Verlag GmbH & Co. KGaA, Weinheim.

Fischer-Tropsch synthesis (FTS) is an extensively investigated technique to directly convert syngas into light olefins, but this process suffers from low selectivity (58% for C_2–C_4) and serious carbon deposition.[77] Jiao *et al.*[16] reported the unprecedented high selectivity on the basis of a novel OX-ZEO process, as high as 80% for $C_2^=$–$C_4^=$ and up to 94% for C_2–C_4 with the CO conversion of 17%. SVUV-PIMS at HLS-II was used to detect the gas-phase intermediates and products in syngas conversion over $ZnCrO_x$. A series of products were observed in mass spectra, among which the most important intermediate ketene was identified by comparing the mass spectra recorded at different photon energies (Fig. 9). Based on the experimental observation and DFT calculations, a unique ketene-involved mechanism was proposed, in which CO and H_2 are activated on the partially reduced oxide surface ($ZnCrO_x$) with the formation of ketene, and ketene was transported in the gas phase to the active sites of MSAPO, where they were converted into olefins. This mechanism indicates the activation of syngas, and the production of olefins is activated by different active sites, which is quite different from the surface polymerization of CH_x intermediates in the generally accepted FTS reaction mechanism.

4.3 Key intermediates in MTH reactions

The MTH process is another important route to produce light olefins and aromatics. The MTH reaction mechanism involves olefin- and aromatic hydrocarbon-based cycles which are connected by hydrogen transfer (HT) and cyclization reactions. Recent studies indicate that formaldehyde (HCHO) may act as an important intermediate and was thought to be generated from MeOH in the MeOH-induced HT pathway and participate in the formation of some oxygenic coke precursors.[78,79] Therefore, knowledge of the behaviour of HCHO during the MTH reaction is important for understanding the HT pathway. Recently, Wen *et al.*[17] successfully detected formaldehyde as a reactive intermediate in the MTH reaction over HSAPO-34 and HZSM-5 at the pressure of 266.6 Pa (Fig. 10). Thanks to the excellent signal response of SVUV-PIMS to formaldehyde, despite the extremely low equilibrium concentration of formaldehyde, the evolution of formaldehyde and other products during the complete reaction process of MTH can be observed in real time. The formation trends of formaldehyde and methane were found to be similar during the MTH process over HSAPO-34, and the yields were closely related, indicating that they are produced by the disproportionation of methanol, and the existence of Y_2O_3 was proven to help decompose formaldehyde and improve the conversion efficiency to hydrocarbons. While for HZSM-5, the yield of formaldehyde was found to affect the formation of dienes, aromatics, coke, and ethylene, which revealed the involvement of formaldehyde during the entire aromatic hydrocarbon-based cycle.

5 Future outlooks

It is very clear that the high photon flux and tunability of SVUV light can afford great selectivity and sensitivity, as well as the isomer-specific capability that is not present in conventional light sources. The combination of SVUV-PIMS and molecular-beam sampling approach has greatly advanced the understanding of combustion and catalytic chemistry, as well as many other fields.

Recently, Hefei Advanced Light Facility (HALF), a fourth-generation synchrotron light source with a diffraction-limited storage ring, has been proposed and its construction has been started.[80] The radiation will hold the characteristics of transverse coherence and ultra-low divergence angle, which facilitates obtaining smaller light spots with much higher photon intensity at the experimental endstation. This will provide new opportunities for innovation of synchrotron-based experimental methods with higher sensitivity, higher repetition rate, higher spatial resolution and suitable for harsher reaction conditions. Future applications will focus on energy chemistry-related fields,

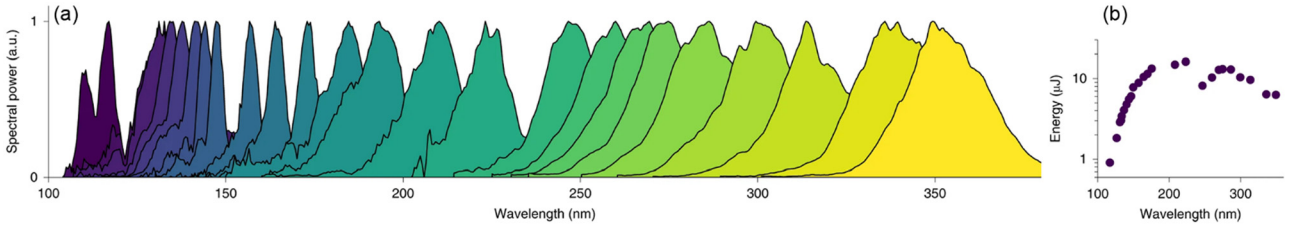

Fig. 11 Tunable RDW emissions in gas-filled HCFs. (a) Measured RDW spectra from a 3-m-long HCF with a 126 μm core radius filled with helium and pumped with 10 fs pulses. (b) Measured pulse energies.[84] Adapted and reproduced with permission from Springer Nature.

such as combustion chemistry at high pressures, homogeneous and heterogenous catalytic chemistry, and aerosol chemistry. Life science and interstellar chemistry will also be covered.

While synchrotron VUV beamlines offer significant advantages over conventional light sources, the access to beam-time at synchrotron facilities is highly competitive and restricted, which is perhaps the greatest limitation in utilizing such advanced approaches. From this point of view, mass spectrometry with conventional VUV light sources will continue to be an essential topic. Actually, VUV light sources including lamps and lasers have already been extensively used for PIMS but are not comparable to synchrotron radiation in terms of high photon flux and tunability. It is difficult for conventional lamp-based light sources to achieve high photon flux, except for a light source named electron beam pumped excimer light (EBEL), which can deliver a photon flux of up to 3×10^{17} photons s^{-1}.[81,82] Several typical wavelengths such as 122 nm, 124 nm, and 126 nm can be obtained by replacing the gas filling. Zimmermann's group has carried out a large number of impressive applications with EBEL. On the other hand, lasers can also generate VUV light through four-wave mixing, high-harmonics and nonlinear optics but it suffers from the limited gaps of tunability and time-consuming operation. Notable progress is the recently developed VUV light sources based on optical soliton dynamics in large-core hollow capillary fibres (HCFs).[83,84] For example, Travers and co-workers reported the efficient generation of VUV pulses in the range of 110–400 nm through resonant dispersive-wave emission (RDW).[84] The biggest advantage of this technology is the simultaneous achievement of continuous tunability and high intensity on a bench-top light source. The energy is reported approximately 1 μJ in the range of 107–121 nm, and 13 μJ near 180 nm (Fig. 11). These superior characteristics may enable the resolution of isomers beyond the ability of current synchrotron-based photoionization facilities, which is essential for serving the broader scientific community.

Conflicts of interest

There are no conflicts to declare.

Acknowledgements

This work was supported by the National Key R&D Program of China (2019YFA0405600).

References

1 K. Kohse-Hoinghaus, *Proc. Combust. Inst.*, 2021, **38**, 1–56.
2 W. Yuan, Y. Li and F. Qi, *Sci. China: Chem.*, 2017, **60**, 1391–1401.
3 Z. Wang, O. Herbinet, N. Hansen and F. Battin-Leclerc, *Prog. Energy Combust. Sci.*, 2019, **73**, 132–181.
4 F. N. Egolfopoulos, N. Hansen, Y. Ju, K. Kohse-Hoinghaus, C. K. Law and F. Qi, *Prog. Energy Combust. Sci.*, 2014, **43**, 36–67.
5 F. Qi, *Proc. Combust. Inst.*, 2013, **34**, 33–63.
6 N. Hansen, T. A. Cool, P. R. Westmoreland and K. Kohse-Hoinghaus, *Prog. Energy Combust. Sci.*, 2009, **35**, 168–191.
7 C. A. Taatjes, N. Hansen, D. L. Osborn, K. Kohse-Hoinghaus, T. A. Cool and P. R. Westmoreland, *Phys. Chem. Chem. Phys.*, 2008, **10**, 20–34.
8 T. A. Cool, K. Nakajima, T. A. Mostefaoui, F. Qi, A. McIlroy, P. R. Westmoreland, M. E. Law, L. Poisson, D. S. Peterka and M. Ahmed, *J. Chem. Phys.*, 2003, **119**, 8356–8365.
9 T. A. Cool, A. McIlroy, F. Qi, P. R. Westmoreland, L. Poisson, D. S. Peterka and M. Ahmed, *Rev. Sci. Instrum.*, 2005, **76**, 094102.
10 F. Qi, R. Yang, B. Yang, C. Huang, L. X. Wei, J. Wang, L. Sheng and Y. Zhang, *Rev. Sci. Instrum.*, 2006, **77**, 084101.
11 P. Oßwald, P. Hemberger, T. Bierkandt, E. Akyildiz, M. Köhler, A. Bodi, T. Gerber and T. Kasper, *Rev. Sci. Instrum.*, 2014, **85**, 025101.
12 Z. Zhou, H. Guo and F. Qi, *TrAC, Trends Anal. Chem.*, 2011, **30**, 1400–1409.
13 C. A. Taatjes, N. Hansen, A. McIlroy, J. A. Miller, J. P. Senosiain, S. J. Klippenstein, F. Qi, L. S. Sheng, Y. W. Zhang, T. A. Cool, J. Wang, P. R. Westmoreland, M. E. Law, T. Kasper and K. Kohse-Hoinghaus, *Science*, 2005, **308**, 1887–1889.
14 Z. Wang, D. M. Popolan-Vaida, B. Chen, K. Moshammer, S. Y. Mohamed, H. Wang, S. Sioud, M. A. Raji, K. Kohse-Hoinghaus, N. Hansen, P. Dagaut, S. R. Leone and S. M. Sarathy, *Proc. Natl. Acad. Sci. U. S. A.*, 2017, **114**, 13102–13107.
15 F. Battin-Leclerc, O. Herbinet, P. A. Glaude, R. Fournet, Z. Zhou, L. Deng, H. Guo, M. Xie and F. Qi, *Angew. Chem., Int. Ed.*, 2010, **49**, 3169–3172.
16 F. Jiao, J. Li, X. Pan, J. Xiao, H. Li, H. Ma, M. Wei, Y. Pan, Z. Zhou, M. Li, S. Miao, J. Li, Y. Zhu, D. Xiao, T. He, J. Yang, F. Qi, Q. Fu and X. Bao, *Science*, 2016, **351**, 1065–1068.

17 W. Wen, S. Yu, C. Zhou, H. Ma, Z. Zhou, C. Cao, J. Yang, M. Xu, F. Qi, G. Zhang and Y. Pan, *Angew. Chem., Int. Ed.*, 2020, **59**, 4873–4878.
18 M. Ahmed and O. Kostko, *Phys. Chem. Chem. Phys.*, 2020, **22**, 2713–2737.
19 J. Wang, Y. Y. Li, T. C. Zhang, Z. Y. Tian, B. Yang, K. W. Zhang, F. Qi, A. G. Zhu, Z. F. Cui and C. Y. Ng, *Astrophys. J.*, 2008, **676**, 416–419.
20 R. I. Kaiser, L. Zhao, W. Lu, M. Ahmed, V. S. Krasnoukhov, V. N. Azyazov and A. M. Mebel, *Nat. Commun.*, 2022, **13**, 786.
21 L. Zhao, R. I. Kaiser, W. Lu, B. Xu, M. Ahmed, A. N. Morozov, A. M. Mebel, A. H. Howlader and S. F. Wnuk, *Nat. Commun.*, 2019, **10**, 3689.
22 Z. Zhou, X. Du, J. Yang, Y. Wang, C. Li, S. Wei, L. Du, Y. Li, F. Qi and Q. Wang, *J. Synchrotron Radiat.*, 2016, **23**, 1035–1045.
23 X. Du, C. Li, S. Wei, L. Du, J. Yang, Z. Zhou, F. Qi and Q. Wang, *AIP Conf. Proc.*, 2016, **1741**, 030037.
24 Z. Zhou, J. Yang, Y. Pan and F. Qi, *J. Chin. Mass Spectrom. Soc.*, 2021, **42**, 598–608.
25 Z. Zhou, in *Encyclopedia of Analytical Science* Third Edition, ed. P. Worsfold, C. Poole, A. Townshend and M. Miró, Academic Press, Oxford, 2019, DOI: **10.1016/B978-0-12-409547-2.14008-9**, pp. 483–490.
26 L. Hanley and R. Zimmermann, *Anal. Chem.*, 2009, **81**, 4174–4182.
27 J. C. Biordi, *Prog. Energy Combust. Sci.*, 1977, **3**, 151–173.
28 S. R. Leone, M. Ahmed and K. R. Wilson, *Phys. Chem. Chem. Phys.*, 2010, **12**, 6564–6578.
29 C. Liu, L. Ye, W. Yuan, Y. Zhang, J. Zou, J. Yang, Y. Wang, F. Qi and Z. Zhou, *Fuel*, 2018, **232**, 632–638.
30 W. Chen, Q. Xu, H. Lou, Q. Di, C. Xie, B. Liu, J. Yang, H. Le Gall, L. S. Tran, X. Wang, Z. Xia, O. Herbinet, F. Battin-Leclerc and Z. Wang, *Combust. Flame*, 2022, **240**, 111946.
31 R. You, S. Yu, J. Yang, Y. Pan and W. Huang, *Rev. Sci. Instrum.*, 2020, **91**, 093102.
32 T. A. Cool, K. Nakajima, C. A. Taatjes, A. McIlroy, P. R. Westmoreland, M. E. Law and A. Morel, *Proc. Combust. Inst.*, 2005, **30**, 1681–1688.
33 Y. Li, L. Zhang, Z. Tian, T. Yuan, J. Wang, B. Yang and F. Qi, *Energy Fuels*, 2009, **23**, 1473–1485.
34 J. C. Person, *J. Chem. Phys.*, 1965, **43**, 2553–2555.
35 J. C. Person and P. P. Nicole, *J. Chem. Phys.*, 1968, **49**, 5421–5426.
36 J. C. Person and P. P. Nicole, *J. Chem. Phys.*, 1970, **53**, 1767–1774.
37 J. C. Person and P. P. Nicole, *J. Chem. Phys.*, 1971, **55**, 3390–3397.
38 T. A. Cool, J. Wang, K. Nakajima, C. A. Taatjes and A. McIlroy, *Int. J. Mass Spectrom.*, 2005, **247**, 18–27.
39 C. A. Taatjes, S. J. Klippenstein, N. Hansen, J. A. Miller, T. A. Cool, J. Wang, M. E. Law and P. R. Westmoreland, *Phys. Chem. Chem. Phys.*, 2005, **7**, 806–813.
40 Z. Zhou, M. Xie, Z. Wang and F. Qi, *Rapid Commun. Mass Spectrom.*, 2009, **23**, 3994–4002.
41 T. Adam and R. Zimmermann, *Anal. Bioanal. Chem.*, 2007, **389**, 1941–1951.
42 Z. Zhou, L. Zhang, M. Xie, Z. Wang, D. Chen and F. Qi, *Rapid Commun. Mass Spectrom.*, 2010, **24**, 1335–1342.
43 M. Xie, Z. Zhou, Z. Wang, D. Chen and F. Qi, *Int. J. Mass Spectrom.*, 2010, **293**, 28–33.
44 M. Xie, Z. Zhou, Z. Wang, D. Chen and F. Qi, *Int. J. Mass Spectrom.*, 2011, **303**, 137–146.
45 M. S. Eschner and R. Zimmermann, *Appl. Spectrosc.*, 2011, **65**, 806–816.
46 H. Jin, J. Yang and A. Farooq, *Rapid Commun. Mass Spectrom.*, 2020, **34**, e8899.
47 J. Yang, *Photonionization Cross Section Database (Version 2.0)*, 2017, **https://flame.nsrl.ustc.edu.cn/database/**.
48 R. R. Lucchese and V. McKoy, *J. Phys. Chem.*, 1981, **85**, 2166–2169.
49 R. R. Lucchese, G. Raseev and V. McKoy, *Phys. Rev. A: At., Mol., Opt. Phys.*, 1982, **25**, 2572–2587.
50 F. A. Gianturco, R. R. Lucchese and N. Sanna, *J. Chem. Phys.*, 1994, **100**, 6464–6471.
51 A. P. P. Natalense and R. R. Lucchese, *J. Chem. Phys.*, 1999, **111**, 5344–5348.
52 K. Moshammer, A. W. Jasper, D. M. Popolan-Vaida, Z. D. Wang, V. S. B. Shankar, L. Ruwe, C. A. Taatjes, P. Dagaut and N. Hansen, *J. Phys. Chem. A*, 2016, **120**, 7890–7901.
53 J. Huang, C. Huang, X. Wu, Q. Hou, G. Tian, J. Yang and F. Zhang, *J. Chem. Phys.*, 2021, **154**, 244301.
54 J. Huang, X. Wu, Q. Hou, M. Wu, J. Yang and F. Zhang, *Energy Fuels*, 2021, **35**, 14051–14062.
55 B. Yang, P. Oßwald, Y. Li, J. Wang, L. Wei, Z. Tian, F. Qi and K. Kohse-Höinghaus, *Combust. Flame*, 2007, **148**, 198–209.
56 Z. Wang, L. Zhang, K. Moshammer, D. M. Popolan-Vaida, V. S. B. Shankar, A. Lucassen, C. Hemken, C. A. Taatjes, S. R. Leone, K. Kohse-Hoinghaus, N. Hansen, P. Dagaut and S. M. Sarathy, *Combust. Flame*, 2016, **164**, 386–396.
57 Z. Wang and S. M. Sarathy, *Combust. Flame*, 2016, **165**, 364–372.
58 J. Zou, X. Zhang, Y. Li, L. Ye, L. Xing, W. Li, C. Cao, Y. Zhai, F. Qi and J. Yang, *Combust. Flame*, 2020, **214**, 211–223.
59 J. Zou, H. Jin, D. Liu, X. Zhang, H. Su, J. Yang, A. Farooq and Y. Li, *Combust. Flame*, 2022, **235**, 111550.
60 J. Zou, Y. Li, L. Ye and H. Jin, *Combust. Flame*, 2022, **235**, 111658.
61 J. Zou, J. Zhang, T. Lian, Q. Xu, B. Liu, Z. Wang, J. Yang and Y. Li, *Combust. Flame*, 2022, DOI: **10.1016/j.combustflame.2021.111963**.
62 H. Wang and M. Frenklach, *J. Phys. Chem.*, 1994, **98**, 11465–11489.
63 D. S. N. Parker, F. Zhang, Y. S. Kim, R. I. Kaiser, A. Landera, V. V. Kislov, A. M. Mebel and A. G. G. M. Tielens, *Proc. Natl. Acad. Sci. U. S. A.*, 2012, **109**, 53–58.
64 L. Zhao, M. B. Prendergast, R. I. Kaiser, B. Xu, U. Ablikim, M. Ahmed, B.-J. Sun, Y.-L. Chen, A. H. H. Chang, R. K. Mohamed and F. R. Fischer, *Angew. Chem., Int. Ed.*, 2019, **58**, 17442–17450.
65 K. O. Johansson, M. P. Head-Gordon, P. E. Schrader, K. R. Wilson and H. A. Michelsen, *Science*, 2018, **361**, 997–1000.
66 H. Jin, L. Xing, J. Yang, Z. Zhou, F. Qi and A. Farooq, *J. Phys. Chem. Lett.*, 2021, **12**, 8109–8114.

67 H. Jin, L. Ye, J. Yang, Y. Jiang, L. Zhao and A. Farooq, *J. Am. Chem. Soc.*, 2021, **143**, 20710–20716.
68 H. Kobayashi, A. Hayakawa, K. D. Kunkuma, A. Somarathne and E. C. Okafor, *Proc. Combust. Inst.*, 2019, **37**, 109–133.
69 P. Glarborg, J. A. Miller, B. Ruscic and S. J. Klippenstein, *Prog. Energy Combust. Sci.*, 2018, **67**, 31–68.
70 W. Yuan, L. Ruwe, S. Schwarz, C. Cao, J. Yang, O. Deutschmann, K. Kohse-Höinghaus and F. Qi, *Proc. Combust. Inst.*, 2021, **38**, 795–803.
71 L. Luo, X. Tang, W. Wang, Y. Wang, S. Sun, F. Qi and W. Huang, *Sci. Rep.*, 2013, **3**, 1625.
72 L. Luo, R. You, Y. Liu, J. Yang, Y. Zhu, W. Wen, Y. Pan, F. Qi and W. Huang, *ACS Catal.*, 2019, **9**, 2514–2520.
73 S. Arndt, G. Laugel, S. Levchenko, R. Horn, M. Baerns, M. Scheffler, R. Schlögl and R. Schomäcker, *Catal. Rev.*, 2011, **53**, 424–514.
74 J. Sadeghzadeh Ahari, S. Zarrinpashne and M. T. Sadeghi, *Fuel Process. Technol.*, 2013, **115**, 79–87.
75 Y. Simon, F. Baronnet and P.-M. Marquaire, *Ind. Eng. Chem. Res.*, 2007, **46**, 1914–1922.
76 N. R. Farooji, A. Vatani and S. Mokhtari, *J. Nat. Gas Chem.*, 2010, **19**, 385–392.
77 H. M. Torres Galvis and K. P. de Jong, *ACS Catal.*, 2013, **3**, 2130–2149.
78 S. Müller, Y. Liu, F. M. Kirchberger, M. Tonigold, M. Sanchez-Sanchez and J. A. Lercher, *J. Am. Chem. Soc.*, 2016, **138**, 15994–16003.
79 X. Sun, S. Mueller, Y. Liu, H. Shi, G. L. Haller, M. Sanchez-Sanchez, A. C. van Veen and J. A. Lercher, *J. Catal.*, 2014, **317**, 185–197.
80 L. Wang, W. Li, Q. Luo, H. Li, Y. Lu, G. Liu, S. Zhang, W. Xu, P. Yang, N. Hu, D. Xu, Z. Bai and Z. Yang, *9th International Particle Accelerator Conference*, Vancouver, BC, Canada, 2018, DOI: **10.18429/JACOW-IPAC2018-THPMK120**.
81 J. Wieser, A. Morozov, F. Muhlberger, R. Zimmermann and A. Ulrich, in *Atomic and Molecular Pulsed Lasers V*, ed. V. F. Tarasenko, G. V. Mayer and G. G. Petrash, 2004, vol. 5483, pp. 287–291.
82 F. Muhlberger, J. Wieser, A. Ulrich and R. Zimmermann, *Anal. Chem.*, 2002, **74**, 3790–3801.
83 P. S. J. Russell, P. Hölzer, W. Chang, A. Abdolvand and J. C. Travers, *Nat. Photonics*, 2014, **8**, 278–286.
84 J. C. Travers, T. F. Grigorova, C. Brahms and F. Belli, *Nat. Photonics*, 2019, **13**, 547–554.